Anisotropic Thermal Expansion as the Source of Macroscopic and Molecular Scale Motion in Phosphorescent Amphidynamic Crystals

Mingoo Jin,[a,c] Sho Yamamoto,[b] Tomohiro Seki,[b] Hajime Ito*[b,c] and Miguel A. Garcia-Garibay*[a]

Abstract: The structural origin of multiscale phenomena, with physical manifestations ranging from the molecular to the macroscopic scale, remains largely undocumented. Here we report the discovery of a crystalline molecular rotor with rotationally-modulated triplet emission that displays macroscopic dynamics in the form of crystal moving and/or jumping, also known as salient effects. Crystals of molecular rotor **2** with a central 1,4-diethynyl-2,3-difluorophenylene rotator linked to two gold(I) nodes, which crystalizes as infinite 1D chains by taking advantage of intermolecular gold(I)-gold(I) interactions. It was shown that rotational motion leads to changes in the orientation of the central phenylene, causing changes in electronic communication between adjacent chromophores, which are manifested as changes in emission intensities. Crystals of **2** showed the large and reversible thermal expansion/compression anisotropy, which was shown to account for (1) a nonlinear Arrhenius behavior in molecular-level rotational dynamics, which correlates with (2) changes in emission, and determines (3) the macroscopic crystal motion. Furthermore, a molecular rotor analog **3** possessing a 1,4-diethynyl-2,3,5,6-tetrafluorophenylene rotator exhibited unit cell anisotropy, crystal dynamics, emission properties and thermosalience that are similar to those of **2**, suggesting potentially generalizable new avenues to control mechanical properties at the molecular and macroscopic scales.

The design of molecular machines with applications in the macroscopic world remains a major challenge.[1-12] We and others have addressed it by exploring the emergent properties of amphidynamic crystals, which are built with a combination of lattice forming elements and moving parts.[9-24] To date, examples have been reported of amphidynamic crystals with the potential of controlling gas adsorption and desorption,[12,15] electric,[25-28,33] optic,[29,30] shape memory,[31-33] and luminescence,[35-38] among other properties.[9-12]

[a] Dr. M. Jin, and Prof. Dr. M.A. Garcia-Garibay
University of California Los Angeles, Department of Chemistry & Biochemistry, California 90095-1569, United States.
E-mail: mgg@chem.ucla.edu
[b] Mr. S. Yamamoto, Dr. T. Seki, and Prof. Dr. H. Ito
Division of Applied Chemistry and Frontier Chemistry Center (FCC), Faculty of Engineering, Hokkaido University, Sapporo, Hokkaido 060-8628, Japan
[c] Assistant Prof. Dr. M. Jin, and Prof. Dr. H. Ito
Institute for Chemical Reaction Design and Discovery (WPI-ICReDD), Hokkaido University, Sapporo, Hokkaido, 060-8628, Japan

Supporting information for this article is given via a link at the end of the document.

One of the most robust molecular architectures for the formation of amphidynamic crystals is based on the use of dumbbell shaped molecular rotors.[9,10,12] Their structures are generally based on a central phenylene rotator linked by a dialkyne axle to bulky groups that build up the lattice and play the role of a stator. Amphidynamic crystals possess a relatively low packing density and/or a relatively fluid region near the rotator, which makes it possible for fast molecular rotation to occur in the solid state. With that in mind we recently designed an amphidynamic crystal with rotationally-controlled phosphorescence by incorporating a gold(I) complex within the dumbbell shaped motif in complex **1** (Figure 1a).[35] We were aware that analogous structures tend to have aurophilic interactions between the adjacent gold(I) complexes in the crystal [gold(I)–gold(I) < 3.5 Å], suggesting that rotation of the central phenylenes would be able to alter the electronic communication between units.

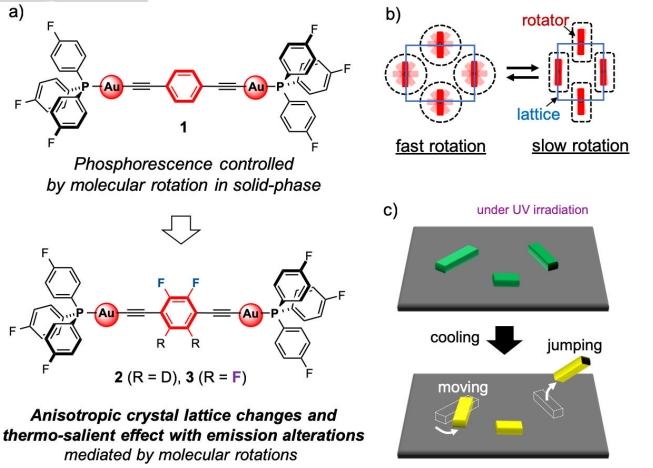

Figure 1. a) Isosteric substitution of the central phenylene rotator in complex **1** by a 2,3-difluorophenylene (**2**) or a tetra-fluorophenylene (**3**). b) Representation of the anisotropic crystal lattice expansion/compression and its potential effect on molecular rotation. c) Illustration of the observed thermo-salient effects with emission color changes of crystals **2** and **3**.

We also reasoned that changes in the electronics of the complex as a function of rotational motion could be manifested in the form of changes in emission properties. As expected, changes in triplet emission in crystals of **1** were correlated with changes in the thermally-induced rotational motion of the central phenylenes.[35] As the next step in our efforts to prepare stimuli-responsive crystalline materials, we decided to prepare and analyze the properties of the analogous isomorphic structure of complex **2**, which has a polar 2,3-difluorophenylene rotator (Figure 1a). Notably, during the process of characterizing this new material we discovered that it displays thermosalient

properties, with crystals displaying temperature-induced macroscopic displacements and jumping motion (Figure 1c). In fact, there have been an increasing number of examples where macroscopic mechanical motion, or "salient effects" can be observed upon exposure of crystals to selected stimuli.[39-44] It has been shown that abrupt changes in unit cell dimensions brought about by chemical reactions, phase transitions, or large thermal expansion coefficients may result in crystal bending, twisting, and/or jumping.[39-41] This creates opportunities to transduce molecular-level events into the macroscopic world.[3b]

In this article we report the preparation and characterization of complex **2** and its tetrafluoro analog **3**, which were shown to be thermosalient. In addition to thermal analysis, we carried out single crystal X-ray diffraction and solid state NMR as function of temperature to investigate the origins of the macroscopic motion, and determine whether or not those changes correlate with rotational dynamics. We showed that these crystals do not undergo a phase transition and confirmed a significant anisotropy in their thermal expansion coefficients (Figure 1b), which correlated with a strongly nonlinear Arrhenius behavior in the case of fluorophenylene rotator **2**, and significant changes in the phosphorescence properties of both **2** and **3**.

Results and Discussion

Dumbbell-shaped gold complexes **2** and **3** were synthesized from derivatives of 1,4-diethynylbenzene and tris(4-fluorophenyl)phosphane gold(I) chloride using standard alkynylation conditions, as illustrated in Scheme 1.[35] Samples of **2** prepared with a deuterated 2,3-difluorophenylene rotator were used to investigate the rotational exchange dynamics using solid state (SS) spin echo ^{2}H-NMR line shape analysis. The gold(I) complex **3** was prepared in a similar manner using tetra-fluorophenylene as a central rotator. Crystallizations of complexes **2** and **3** were carried out by layering MeOH as an anti-solvent on top of a solution of the corresponding rotor complex in dichloromethane (typically, 5 mg of the complexes in 0.2 ml of dichloromethane). Green yellowish single crystals (below 0.5 mm in size) were subsequently shown to emit green phosphorescence under UV light at room temperature. No solvent inclusion was observed in either crystal by X-Ray diffraction or thermogravimetric analysis (TGA) (Figure 2 and S1). Samples were characterized by ^{1}H and ^{13}C NMR spectroscopy, high-resolution mass spectrometry, elemental analysis, TGA, and single crystal X-ray diffraction (XRD) (see the Supporting Information). As described in more detail below, thermosalience was first observed during variable temperature emission measurements of molecular rotor complexes **2** and **3**.

Gold(I) complex **2** crystallized in the monoclinic space group *I2/a* with four molecules generated in the unit cell (Z=4) (Table S1). We confirmed our expectation that solid state structure of **2** would be isostructural to that of **1** with infinite zigzag chains determined by inter-molecular aurophilic interactions between neighboring molecular rotors. Intermolecular gold(I)–gold(I) distances of 3.0299(7) Å were observed (Figure 2a-b and S2). The two-fold rotationally disordered difluorophenylenes are surrounded by fluorophenyl groups from the phosphane stators of neighboring gold(I) complexes, which also present some local disorder (Figure 2b and S2).

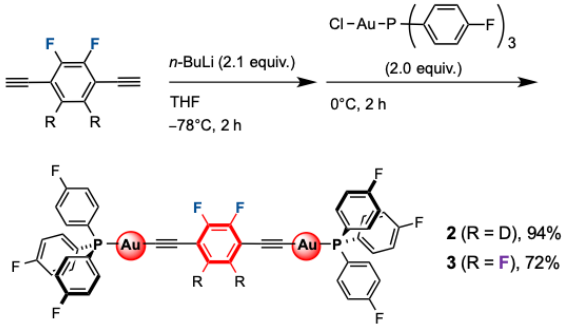

Scheme 1. Synthetic scheme of the gold(I) complexes **2** and **3**.

Crystals of Gold(I) complex **3** with a central tetrafluoro phenylene were obtained in the monoclinic space group *P2/c* (Table S2). The intermolecular zigzag chains and packing environment near the rotator in crystal **3** were very similar to those of **2** (Figure 2d and S3), suggesting that the tetrafluoro phenylene rotator of **3** would be likely to display similar rotational motion (Figure 2d-e and S3). Crystals of **3** have four molecule per unit cell (*Z*=4) (Table S1) with neighboring molecules experiencing gold(I)–gold(I) distances of 3.1016(9) Å and 2.9522(9) Å (Figure 2d-e). The slight difference in aurophilic interactions between crystal **2** and **3** resulted the different space groups even though both crystals forms have very similar packing structures As shown respectively in Figures 2e and 2f, the tetrafluoro phenylene rotators of **3** are surrounded by fluorophenyl groups of neighboring stators and the plane of the central rotator coincides the *b*/*c*-plane.

In order to explore possible changes in the packing structure that may explain the macroscopic crystal and molecular rotary dynamics of the two molecular rotor complexes, we carried out XRD measurements in the temperature range from 123 K to 298 K with eight intermediate steps at 153, 173, 193, 213, 233, 253, and 273 K. No significant phase transitions were observed and changes in gold(I)–gold(I) distances between 123 and 298 K were less than 0.058 Å (Figure S4 and S5). However, both crystals displayed a significant expansion/compression anisotropy as a function of temperature. As shown in Figure 2g-l, the direction of the largest change in each crystal corresponds to the axis orthogonal to the planes of rotation of the fluorinated phenylenes, which is the a-axis in the case of **2** and the c-axis in the case of **3**. Based on these results, it is reasonable to expect that these anisotropic lattice changes would affect the motion of the central aryl rings. Differential scanning calorimetry (DSC) profiles of both crystals, measured at a heating rate of 10 K/min, showed no significant peaks in the range 153–298 K, indicating that these crystals have no thermally triggered martensic phase transitions (Figure S6-7).

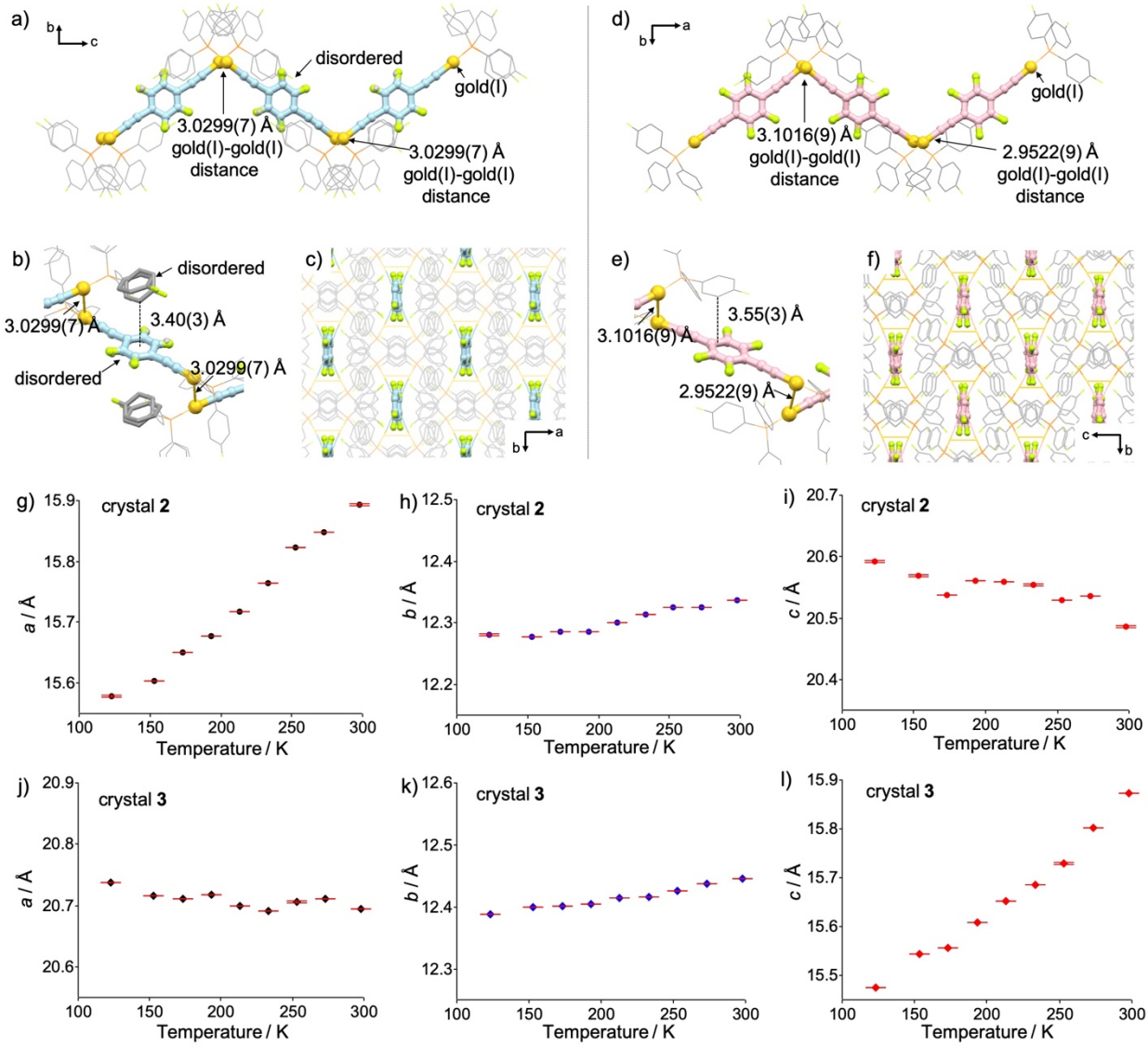

Figure 2. Crystal structures of **2** and **3** with the tris(4-fluorophosphane) ligands shown in light grey and 1,4-di-gold(I)ethynyl benzene units highlighted with colored thick bars and atoms. Zigzag intermolecular networks formed by dimeric aurophilic interactions in a) **2** and d) **3**. Dimeric aurophilic interaction distances between neighboring molecular rotors in complexes b) **2** and e) **3**. Rotator arrangements in crystals c) **2** and f) **3** viewed down the c-axis and a-axis, respectively. Plots of the unit cell parameters of crystals g), h), i) **2** and j), k), l) **3** versus the measured temperatures (standard deviation in temperature values are shown in horizontal red bars).

In order to investigate the rotational dynamics of gold(I) rotor **2** we carried out solid state (SS) ^{2}H NMR spin-echo measurements and line shape simulations. This technique is widely used to analyze internal dynamics of deuterium-enriched groups with exchange rates in the range of ca. 10^{3}–10^{7} Hz.[45] The measurements were performed on powdered (crushed) single crystals of **2** to determine the rotational frequency of the central phenylene as a function of temperature.[46] Figure 3a shows the experimental spectra measured in the range between 318 K and 193 K in solid black lines. Line shapes obtained by simulation shown as red dotted lines provided a reasonably match with those obtained in the experiment. The calculated spectra were obtained using a quadrupolar coupling constant (QCC) of 180 kHz[45] that is characteristic of aromatic deuterons, a cone angle of 60° formed between the rotational 1,4-axis and C-D bond vector, and Brownian jumps of 180°, in agreement with the crystal structure. The line shape at 318 K is in the intermediate exchange regime and was simulated with a rotational frequency of 2.0 MHz. Spectra measured at 298, 273, 253, 233, 213, and 193 K were simulated with rotational exchange frequencies of ca. 1.35, 1.00, 0.50, 0.20, 0.03, and ≤ 0.01 MHz, respectively (Figure 3a and S7). An Arrhenius plot constructed from the rotational exchange frequencies of **2** presented a significant curvature (Figure 3b), suggesting that the magnitude of the activation energy or the mechanisms for rotation change as a function of temperature. We suggest that the concave downward curvature is consistent with the X-ray data, where the activation energy becomes smaller (Figure 3c) as the size of the unit cell axis that defines the size of the cavity

increases as shown in Figure 2. A rough and qualitative measure of the change in activation accompanying the changes

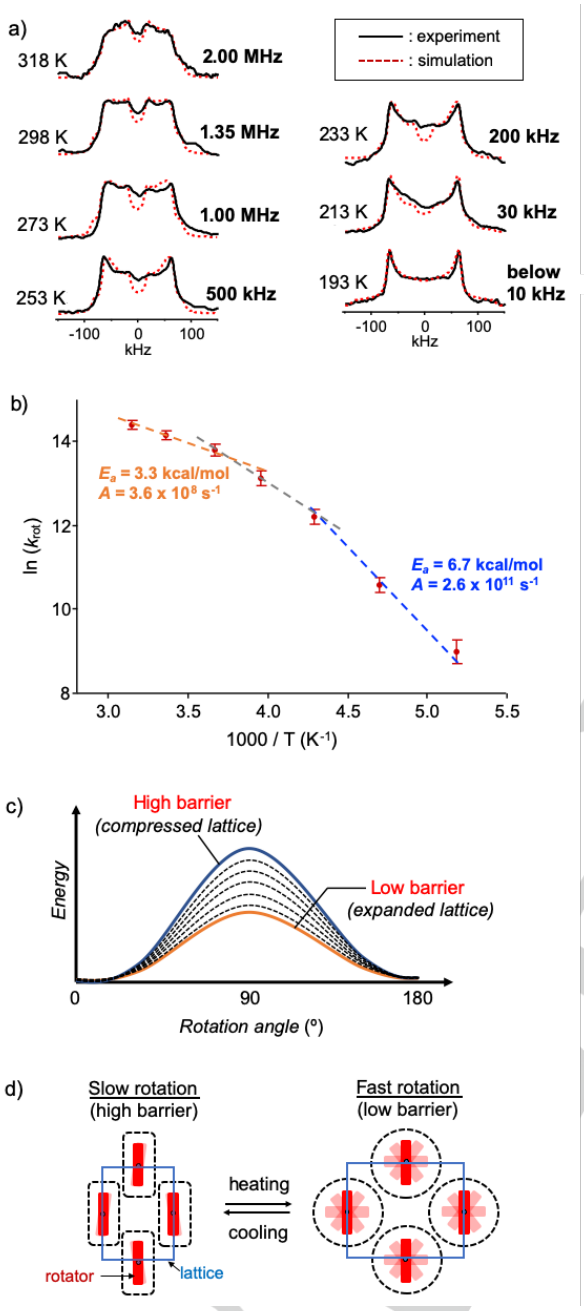

Figure 3. Variable temperature (VT) solid state ^{2}H NMR studies of 2. a) Experimental and simulated SS ^{2}H NMR spectra represented in black solid line and red dashed line, respectively. b) Arrhenius plot of difluorophenylene rotator dynamics in crystal **2** and roughly fitted lines of the high (orange dashed line), intermediate (gray dashed line), and low (blue dashed line) temperature area. c) Hypothetical potential energy diagram for the rotation of the central rotators in crystals **2** and **3**, suggesting changes in activation energy as a result of temperature-induced changes in the size of rotator cavity. d) Schematic representation of the anisotropic expansion/compression and how it correlates with the rotator dynamics as function of temperature.

in unit cell can be obtained by calculating activation parameters in the relatively linear portions of the high and low temperature data, between 193 and 233 K and between 253 and 318 K, respectively. One can estimate low and high temperature barriers in the range of 6.7 kcal/mol and 3.3 kcal/mol, with pre-exponential factors that vary from of 2.6x10^{11} s^{-1} and 3.6x10^8 s^{-1}, respectively (linear fits not shown). It is worth noting that the pre-exponential factor in the low temperature regime is consistent with an elementary dynamic process associated with the frequency of a thermally activated torsional mode that becomes a full rotation, which is expected to be on the order of 10^{12} s^{-1}. By contrast, a low pre-exponential factor in the high temperature region may be viewed as associated with a more complex mechanism and unfavorable activation entropy such as the need for correlated motions. To our knowledge, there are no general theories that relate the pre-exponential factor to structural effects. Our interpretation implies that structural variations resulting from a large anisotropic thermal expansion in the crystal result in significant changes in both the height of the barrier (Figure 3c) and the pre-exponential factor.

To explore the dynamics of the tetra-flourophenylene rotator of gold(I) complex **3**, we carried out variable temperature solid state CPMAS ^{13}C NMR of **3** in the range of 189 K to 302 K. We observed no significant changes in the weak C-F signals assigned to the rotator, which occur as multiplets as a result of one, two and three bond C-F scalar coupling (Figure S9). It is not possible to conclude whether the lack of an observable coalescence process is the result of very slow or static rotation, or the result of insufficient chemical shift differences between the sites related by the postulated two-fold flipping motion. As an alternative, we also carried out solid state ^{19}F NMR measurements at a frequency of 584.686 MHz with polycrystalline samples of **2** and **3** at 193 K and 298 K (Figure 4). While complications arise from the presence of para-fluorine atoms in the triphenylphosphane stator, we found that the ^{19}F NMR spectrum of **2** undergoes line narrowing from values of full width at half maximum (FWHM) that change from ~45 kHz to ~32 kHz in going from 193 K to 298 K, in the same temperature range where ^{2}H NMR reveals rotational exchange frequencies varying from ca. 10 kHz to 1.35 MHz (Figure 3a). Based on the analogies between the spectra of **2** and **3** we proposed that a similar change in line width in the case of **3** from 58 kHz to 40 kHz is supportive of rotational motion in a similar dynamic range.

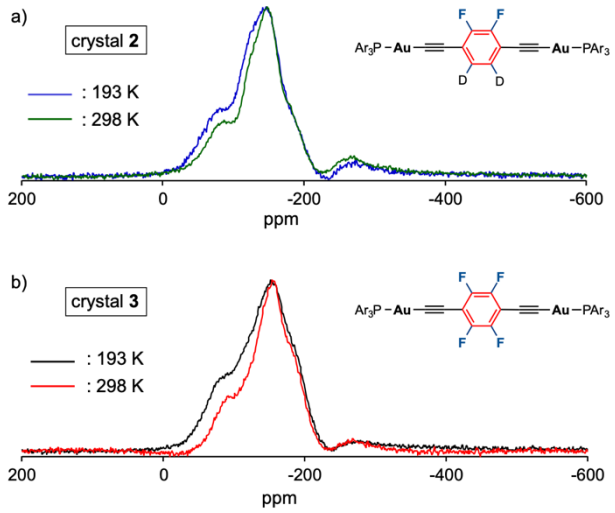

Figure 4. Representative VT ^{19}F NMR spectra of gold(I) complex a) **2** and b) **3**. Line shape broadening were observed between 298 K and 193 K.

With structures that are very similar to that of complex **1**, it seemed reasonable to expect crystals **2** and **3** to have temperature-dependent emission that correlates with their rotational motion. Cooling and heating run under the emission miscroscope were carried out in the range from 298 K to 123 K, which is the same temperature window where the molecular dynamics and crystal structures had been investigated (Figure 5, S9-10, and Supporting movie 1-2). In the first set of experiments described in Figure 6a-f and Supporting movie 1, green emitting crystals **2** were cooled from 298 K to 123 K with a cooling velocity of 40 K/min under UV light illumination. We observed that some crystals experienced small displacements moved at ca. 240–260 K, until they jumped drastically around 220 to 223 K. Crystal jumping or crystal moving were also observed under room light, indicating that the salient effects were not induced by UV light irradiation (Figure S13). Overall, ca. 30% of the crystals in the observation field were found to display macroscopic movement or jumping and crystals **2** showed emission color changes from green to yellow with increased emission intensity upon cooling. When the crystals were heated from 123 to 298 K at the same thermal change speed, the emission recovered its initial color and a few crystals also moved and/or jumped (Figure S11). However, it should be noted that the salient effects were rarely observed during the heating process. We also observed that the second cooling and heating cycle resulted in many fewer jumping and/or moving crystals (Figure S11). Interestingly,

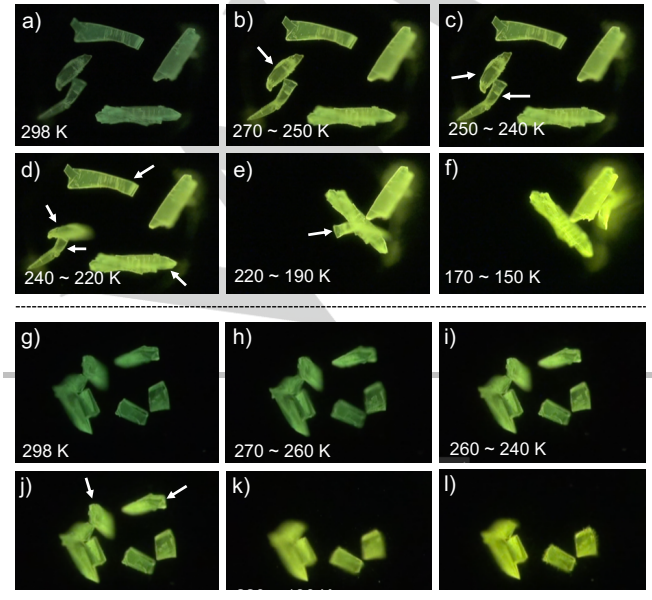

crystals of analog tetrafluoro rotor **3** also exhibited similar thermosalient and emission changes as crystals of difluoro rotor **2** during the cooling and heating process, as described in Figure 5g-l, S12, and Supporting movie 2.

Figure 5. Photographs of the thermo-salient effects with emission color changes of the crystals **2** (a-f) and **3** (g-l) by cooling on 40 K/min, taken under UV light. White arrows indicate the crystals showing the salient behaviors.

There are several examples of thermosalient crystals that experience molecular displacement in their crystal lattice as a result of crystal-to-crystal phase transitions associated with sufficiently large anisotropic unit cell modifications.[39-41,44] As shown in Figure 6, unevenly distributed changes in the crystal lattice caused by a thermal gradient are able to accumulate some stress that, when released, can trigger the observed mechanical response. In the case of **2** and **3**, the anisotropic unit cell compression or expansion during cooling or heating corresponds to the changes in crystal cavity where the rotational motion of the central rotators occurs. The long axis of the crystals **2** and **3** corresponds to a direction orthogonal to the plane of the central rotators, showing the greatest changes in the length as a function of temperature (Figure S14 and S15). As expected, crystal jumping was observed more frequently when cooling with a relatively fast temperature (40 K/min) and no salient effects were observed at all under with cooling rates that are ≤5 K/min.

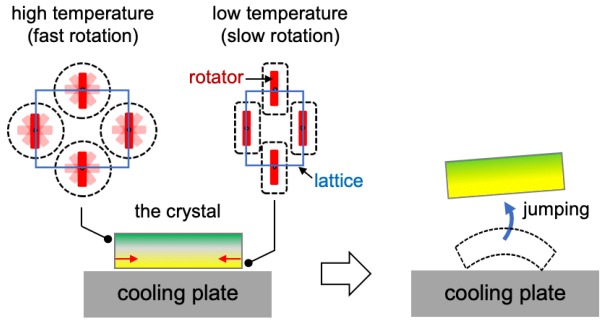

Figure 6. Representation of the expected mechanical motion of crystals **2** and **3** during the thermo-salient effects by the cooling procedure.

As shown in Figure 6 crystals of gold(I) complex **2** exhibited green emission when irradiated with UV light at λ_{ex} = 365 nm at 298 K and similar observations were made for crystal **3**. By contrast, the emission of **2** and **3** in CH_2Cl_2 solution were very weak, as expected for a long-lived phosphorescence that is highly susceptible to quenching by adventitious impurities and residual oxygen (Figure S16 and S17).[35,47] Furthermore, emission lifetimes of crystals **2** and **3** were in the microsecond regime, making it possible to assign it as phosphorescence. The emission spectra of crystalline gold(I) complex **2** has peaks at 503, followed by broad peaks with a maximum at λ_{max} = 547 (Figures 7a). The emission of crystal **3** is completely analogous with corresponding peaks at 507 nm and 551 nm (Figure S18a).

Cooling from 298 to 193 K increased the intensity of the broader red-shifted components (Figure 7a), which corresponds to the color changes that are visually perceived as going from

green to yellow (Figure 5a-f). These observations are consistent with those previously made with crystals of gold(I) complex **1**, which had been shown to correlate with changes in electronic communication caused by changes in the orientation of the central phenyl ring.[35] Notably, changes in the ratio of the emission intensity I_{547}/I_{503} of crystal **2** measured between 298 to 193 K as a function of temperature are complementary to the changes in the a-axis of the unit cell (Figure 7b), which also parallel the changes in rotational motion. A very similar plot obtained for crystal **3** is included in the supporting information section (Figure S18b).

Finally, in order to support a model where changes in emission are modulated by changes in electronic communication that result from the motion of the central rotator, which is akin to dynamic effects behind aggregation induced emission (AIE), [36] we carried out time-dependent (TD) DFT calculations using dimer geometries connected through aurophilic interaction taken from single-crystal structure of **2** and **3** at 193 K. The most important characteristic of the stable rotational ground state structure is that plane of the central aromatic rings are orthogonal to the direction of gold(I)–gold(I) bonds, such that the Aurophilic bonds extend the conjugation between rotators of neighboring molecular rotors. Calculations on the ground state structure confirm that rotation of the difluoro and tetrafluoro-phenylenes within the zigzag chains does affect electronic communication (Figure 8 and S20). Dimer models with the ground state structure (Figure 8, left) and with the central phenylenes rotated by 90° (Figure 8, right) were calculated with B3LYP/SDD method. Vertical excitation energies calculated for the crystal structure had a relatively good agreement with those obtained from the experimental phosphorescence excitation (Figure S19). The frontier molecular orbitals for the dimer with the ground state crystal structure of **2** and **3** indicated that the HOMO and HOMO-1 were distributed over the two diethynyl-fluorobenzenes connected by the aurophilic interaction (Figure 8 bottom left and S20). On the other hand, when these orbitals are calculated with the central phenylene rotated, as shown in Figure 8 (bottom right) and Figure S18, they are completely localized in a one of the two molecular rotors. Interestingly, the LUMO and LUMO+1 of in both cases were mainly located on the tris(4-fluorophenyl)phosphane moiety (Figure 8 top and S20).[35]

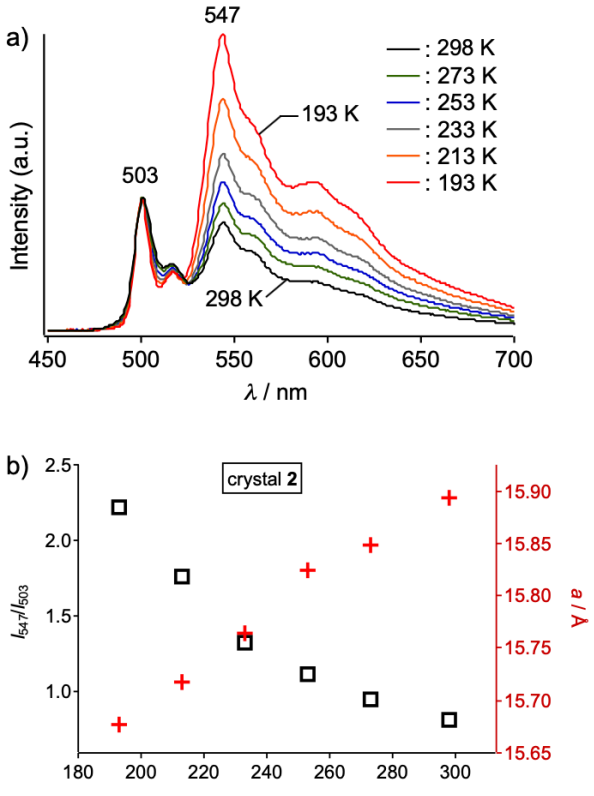

Figure 7. a) Emission spectra of the crystal **2** obtained under UV irradiation (365 nm) as a function of temperature. b) Plots of changes in the ratio of intensity measured at 547 and 503 nm (I_{547}/I_{503}) as a function of temperature (back squares, left axis), and changes in the dimension of the unit cell *a*-axis as a function of temperature in crystal **2** (red crosses, right axis).

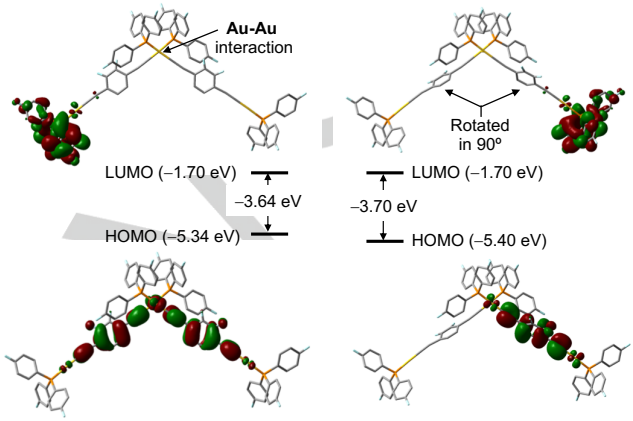

Figure 8. Frontier molecular orbitals and corresponding energy levels obtained by TD-DFT calculation (B3LYP/SDD) of the dimeric structure mediated by aurophilic interaction in crystal **2** (left) and 90° rotated central difluorophenyl ring geometry (right).

The phosphorescence decays of crystals of the gold(I) complexes **2** and **3** were measured at 298, 232, and 195 K in a time window of ca. 100–200 μs (Figure S21 and S22). While emission decays detected near 550 nm displayed high temperature dependence, measurements carried out near 500 nm resulted in multiple components, pointing out to the spectral heterogeneity and kinetic complexity of the solid-state emission (Figure S21and S22). While these emission decays could be fit by models that consider multiple exponential functions with several lifetimes (τ_n) and pre-exponentials (A_n) (Table S8 and S10), their weighted average ($\tau_{av} = \Sigma A_n\tau_n$) varied from ca. 12 μs to 45 μs in the range of 298 to 195 K. From these results, we note that the excitation decay which occurs within the time range for molecular rotations (0.74 μs to 100 μs), which helps explain the high kinetic heterogeneity of the observed emissions and a qualitative correlation between intensity and rotation as a function of temperature, as previously observed in the case of complex **1**.[35] Furthermore, while aurophilic interactions defined by gold(I)–gold(I) distances < 3.5 Å can affect electronic environment of gold(I) complexes, changes in the gold(I)–gold(I) distances of **2** and **3** were below 0.058 Å between 193 to 298 K (Figure S5). Based on these observations, we suggest that phosphorescence changes upon cooling and heating in crystals **2** and **3** are the result of changes in electronic communication that occur when the central aryl plans rotate in the solid state, just as it was suggested in the case of the phosphorescent amphidynamic crystal **1**.

Conclusion

We described here two new examples of multifunctional amphidynamic crystalline materials based on dumbbell complex structures **2** and **3** that are based on ditopic gold(I)complexes linked to a central substituted diethynylphenylene rotator and two triarylphosphanes. Their crystal structures are characterized by molecular rotors linked by aurophilic interactions that form infinite zig-zag chains. The crystalline rotor complexes are characterized by motion at the molecular and macroscopic scales. Macroscopic motion occurs in the form thermosalient crystal moving and/or jumping that is the result of thermal expansion with a relatively large anisotropy. It was shown that thermal expansion occurring on the plane of the rotator increases the free volume and facilitates the rotation, such that the corresponding Arrhenius plots present a significant curvature as the crystal lattice expands. Furthermore, a correlation was observed between phosphorescent properties and rotational motion, which is interpreted in terms of conformational changes that affect the electronic communication between the gold-linked rotors, as supported by DFT studies. The results presented in this article strongly suggest that it may be possible to design chemical structures capable of forming crystalline solids responsive at the macroscopic and molecular scales, including (1) macroscopic polarization by controlling the orientation and rotation of a molecular dipolar array, (2) rotation-mediated emission and other photophysical properties, and (3) thermosalient macroscopic displacement by controlling thermal gradients.

Acknowledgements

This work was financially supported by the MEXT (Japan) program “Strategic Molecular and Materials Chemistry through Innovative Coupling Reactions” of Hokkaido University; Building of Consortia for the Development of Human Resources in Science and Technology, "Program for Fostering Researchers for the Next Generation"; and by JSPS KAKENHI grants JP15H03804, JP16H06034, JP17H05134, JP17H05344, JP17H06370, and JP19K23618. Jin, M. was supported by the grant-in-aid for JSPS Fellows JP17J01104. Work at UCLA was supported by grants National Science Foundation grants DMR-1700471 and MRI-1532232. We thank Dr. Rachel Behrens (The MRL Shared Experimental Facilities in UCSB) for DSC measurements. The MRL Shared Experimental Facilities in UCSB are supported by the MRSEC Program of the NSF under Award No. DMR 1720256; a member of the NSF-funded Materials Research Facilities Network.

Keywords: Molecular rotor • Amphidynamic crystals • Luminescent gold(I) complex

[1] C. Cheng, P. R. McGonigal, S. T. Schneebeli, H. Li, N. A. Vermeulen, C. Ke, J. F. Stoddart, *Nat. Nanotechnol.* **2015,** *10*, 547-553.

[2] M. A.Garcia-Garibay, *Nat. Mater.* **2008**, *7*, 431-432.

[3] a) J. Chen, F. K. Leung, M. C. A. Stuart, T. Kajitani, T. Fukushima, E. van der Giessen, B. L. Feringa, *Nat. Chem.* **2018,** *10*, 132-138. b) A. Colin-Molina, D. P. Karothu, M. J. Jellen, R. A. Toscano, M. A. Garcia-Garibay, P. Naumov, B. Rodriguez-Molina, *Matter*, **2019**,*1*, 1–14.

[4] A. Coskun, M. Banaszak, R. D. Astumian, J. F. Stoddart, B. A. Grzybowski, *Chem. Soc. Rev.* **2012,** *41*, 19-30.

[5] F. Jülicher, A. Ajdari, J. Prost, *Rev. Mod. Phys.* **1997**, *69*, 1269-1281.

[6] M. Guix, C. C. Mayorga-Martinez, A. Merkoci, *Chem. Rev.* **2014,** *114*, 6285-6322.

[7] E. R. Kay, D. A. Leigh, F. Zerbetto, *Angew. Chem. Int. Ed.* **2007,** *46*, 72-191.

[8] R. D. Astumian, *Science* **1997**, *276*, 917-922.

[9] C. S. Vogelsberg, M. A. Garcia-Garibay, *Chem. Soc. Rev.* **2012**, *41*, 1892-1910.

[10] T. A. V. Khuong, J. E. Nuñez, C. E. Godinez, M. A. Garcia-Garibay, *Acc. Chem. Res.* **2006**, *39*, 413-422.

[11] L. Catalano, P. Naumov, *CrystEngComm.* **2018**, *20*, 5872-5883.

[12] A. Comotti, S. Bracco, P. Sozzani, *Acc. Chem. Res.* **2016**, *49*, 1701-1710.

[13] G. M. Lang, T. Shima, L. Wang, K. J. Cluff, K. Skopek, F. Hampel, J. Blümel, J. A. Gladysz, *J. Am. Chem. Soc.* **2016**, *138*, 7649-7663.

[14] W. Setaka, K. Yamaguchi, *J. Am. Chem. Soc.* **2012**, *134*, 12458-12461.

[15] Y. Yan, D. I. Kolokolov, I. da Silva, A. G. Stepanov, A. J. Blake, A. Dailly, P. Manuel, C. C. Tang, S. Yang, M. Schroder, *J. Am. Chem. Soc.* **2017,** *139*, 13349- 13360.

[16] V. N. Vukotic, K. J. Harris, K. Zhu, R. W. Schurko, S. J. Loeb, *Nat. Chem.* **2012**, *4*, 456-460.

[17] C. Lemouchi, C. S. Vogelsberg, L. Zorina, S. Simonov, P. Batail, S. Brown, M. A. Garcia-Garibay, *J. Am. Chem. Soc.* **2011**, *133*, 6371-6379.

[18] X. Jiang, Z. J. O'Brien, S. Yang, L. H. Lai, J. Buenaflor, C. Tan, S. Khan, K. N. Houk, M. A. Garcia-Garibay, *J. Am. Chem. Soc.* **2016,** *138*, 4650-4656.

[19] X. Jiang, B. Rodriguez-Molina, N. Nazarian, M. A. Garcia-Garibay, *J. Am. Chem. Soc.* **2014,** *136*, 8871-8874.

[20] L. Catalano, S. Perez-Estrada, G. Terraneo, T. Pilati, G. Resnati, P. Metrangolo, M. A. Garcia-Garibay, *J. Am. Chem. Soc.* **2015**, *137*, 15386- 15389.

[21] L. Catalano, S. Perez-Estrada, H. H. Wang, A. J. Ayitou, S. I. Khan, G. Terraneo, P. Metrangolo, S. Brown, M. A. Garcia-Garibay, *J. Am. Chem. Soc.* **2017,** *139*, 843-848.

[22] C. S. Vogelsberg, F. J. Uribe-Romo, A. S. Lipton, S. Yang, K. N. Houk, S. Brown, M. A. Garcia-Garibay, *Proc. Nat. Acad. Sci.* **2017**, *114*, 13613- 13618.

[23] W. Li, C. T. He, Y. Zeng, C. M. Ji, Z. Y. Du, W. X. Zhang, X. M. Chen, *J. Am. Chem. Soc.* **2017,** *139*, 8086-8089.

[24] F. Moreau, D. I. Kolokolov, A. G. Stepanov, T. L. Easun, A. Dailly, W. Lewis, A. J. Blake, H. Nowell, M. J. Lennox, E. Besley, S. Yang, M. Schroder, *Proc. Nat. Acad. Sci.* **2017**, *114*, 3056-3061.

[25] T. Akutagawa, H. Koshinaka, D. Sato, S. Takeda, S.-I. Noro, H. Takahashi, R. Kumai, Y. Tokura, T. Nakamura, *Nat. Mater.* **2009**, *8*, 342.

[26] R. D. Horansky, L. I. Clarke, E. B. Winston, J. C. Price, S. D. Karlen, P. D. Jarowski, R. Santillan, M. A. Garcia-Garibay, *Phys. Rev. B* **2006**, *74*, 054306.

[27] J. Y. Liu, S. Y. Zhang, Y. Zeng, X. Shu, Z. Y. Du, C. T. He, W. X. Zhang, X. M. Chen, *Angew. Chem. Int. Ed.* **2018**, *57*, 8032-8036.

[28] J. Harada, M. Ohtani, Y. Takahashi, T. Inabe, *J. Am. Chem. Soc.* **2015**, *137*, 4477-4486.

[29] W. Setaka, K. Yamaguchi, *J. Am. Chem. Soc.* **2013**, *135*, 14560- 14563.

[30] Z. S. Yao, K. Yamamoto, H. L. Cai, K. Takahashi, O. Sato, *J. Am. Chem. Soc.* **2016**, *138*, 12005-12008.

[31] Z. S. Yao, M. Mito, T. Kamachi, Y. Shiota, K. Yoshizawa, N. Azuma, Y. Miyazaki, K. Takahashi, K. Zhang, T. Nakanishi, S. Kang, S. Kanegawa, O. Sato, *Nat. Chem.* **2014,** *6*, 1079-1083.

[32] S. Q. Su, T. Kamachi, Z. S. Yao, Y. G. Huang, Y. Shiota, K. Yoshizawa, N. Azuma, Y. Miyazaki, M. Nakano, G. Maruta, S. Takeda, S. Kang, S. Kanegawa, O. Sato, *Nat. Commun.* **2015,** *6*, 8810.

[33] H.Chung, D. Dudenko, F. Zhang, G. D'Avino, C. Ruzie, A. Richard, G. Schweicher, J. Cornil, D. Beljonne, Y. Geerts, Y. Diao, *Nat. Commun.* **2018,** *9*, 278.
[34] X. Jiang, H. B. Duan, S. I. Khan, M. A. Garcia-Garibay, *ACS Cent Sci* **2016,** *2*, 608-613.
[35] M. Jin, T. S. Chung, T. Seki, H. Ito, M. A. Garcia-Garibay, *J. Am. Chem. Soc.* **2017,** *139*, 18115-18121.
[36] K. Kokado, K. Sada, *Angew. Chem. Int. Ed.* **2019**, *58*, 8632-8639.
[37] a) N. B. Shustova, B. D. McCarthy, M. Dincă, *J. Am. Chem. Soc.* **2011**, *133*, 20126-20129. b) N. B. Shustova, T.-C. Ong, A. F. Cozzolino, V. K. Michalis, R. G. Griffin, M. Dincă, *J. Am. Chem. Soc.* **2012**, *134*, 15061-15070.
[38] M. Hughs, M. Jimenez, S. I. Khan, M. A. Garcia-Garibay, *J. Org. Chem.* **2013**, *78*, 5293-5302.
[39] P. Naumov, S. Chizhik, M. K. Panda, N. K. Nath, E. Boldyreva, *Chem. Rev.* **2015,** *115*, 12440-12490.
[40] P. Commins, I. T. Desta, D. P. Karothu, M. K. Panda, P. Naumov, *Chem. Commun.* **2016,** *52*, 13941-13954.
[41] N. K. Nath, M. K. Panda, S. C. Sahoo, P. Naumov, *CrystEngComm* **2014,** *16*, 1850-1858.
[42] R. Medishetty, S. C. Sahoo, C. E. Mulijanto, P. Naumov, J. J. Vittal, *Chem. Mater.* **2015,** *27*, 1821-1829.
[43] P. Commins, A. Natarajan, C.-K. Tsai, S. I. Khan, N. K. Nath, P. Naumov, M. A. Garcia-Garibay, *Cryst. Growth Des.* **2015,** *15*, 1983-1990.
[44] D. P. Karothu, J. Weston, I. T. Desta, P. Naumov, *J. Am. Chem. Soc.* **2016,** *138*, 13298-13306.
[45] V. Macho, L. Brombacher, H. W. Spiess, *Appl. Magn. Reson.* **2001**, *20*, 405-432.
[46] The powder samples of **2** given by crushing the single crystals were in the same polymorph as the single crystalline specimens, determined by powder XRD patterns, and analogous studies with molecular rotor **3** indicated the same results.
[47] a) J.D. Laposa, H. Singh, *Chem. Phys. Lett.* **1969**, *4*, 288-290. b) L.A. Emmert, W. Choi, J.A. Marshal, Y. Yang, L.A. Meyer, J.A. Brozic, *J. Phys. Chem. A* **2003**, *107*, 11340-11346. c) H.Y. Chao, W. Lu, Y. Li, M.C.W. Chan, C.-M. Che, K.-K. Cheung, N. Zhu, *J. Am. Chem. Soc.* **2002**, *124*, 14696-14706. d) S. Wan, W. Lu, *Angew. Chem. Int. Ed.* **2017**, *56*, 1784-1788.

Entry for the Table of Contents (Please choose one layout)

Layout 1:

RESEARCH ARTICLE

Multifunctional amphidynamic crystalline materials based on dumbbell shape gold(I)complexes are characterized by motion at the molecular and macroscopic scales. Macroscopic motion occurs in the form thermosalient crystal moving and/or jumping that is the result of thermal expansion with a relatively large anisotropy. Furthermore, phosphorescence of the crystals is highly correlated to the molecular rotation.

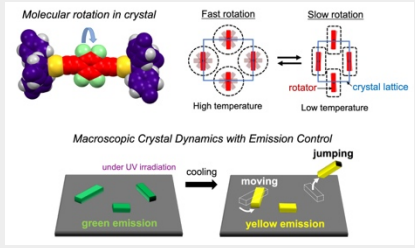

Mingoo Jin, Sho Yamamoto, Tomohiro Seki, Hajime Ito, and Miguel A. Garcia-Garibay**

Page No. – Page No.

Anisotropic Thermal Expansion as the Source of Macroscopic and Molecular Scale Motion in Phosphorescent Amphidynamic Crystals